Vietnam Journal of Catalysis and Adsorption
Tạp chí xúc tác và hấp phụ Việt Nam

http://jca.edu.vn

In situ Growth of Nickel Ferrite Nanoparticles on MXene as High Performance Electromagnetic Wave Absorber in X-Band

Thuy Hao Nguyen[1,2] Sy Duc Dao[1], Duc Thang Do[1], Thi Hoa Nguyen[2], Van Hoanh Ngo[2,*]

[1] *Faculty of Chemistry, University of Science, Vietnam National University, Hanoi, 19 Le Thanh Tong, Hoan Kiem, Ha Noi*
[2] *Institute of Chemistry, Biology and Environment, 17 Hoang Sam, Nghia Do, Hanoi.*
* *Email: nvhchem@gmail.com*

ARTICLE

Received: 01/10/202025
Accepted: 06/12/2025
Published: 30/12/2025

Keywords:
Ti_3C_2 Mxene;
Nickel ferrite nanoparticles;
X-band electromagnetic wave absorption

ABSTRACT

$Ti_3C_2T_x$ MXene sheets - a two-dimensional material with large surface area and high conductivity – show promise in electromagnetic wave (EMW) absorption, however, achieving strong and efficient absorption of electromagnetic waves in the X-band region still faces many challenges. Here, nickel ferrite nanoparticles were grown in situ on the surface and introduced into the interlayers of MXene sheets through a facile co-precipitation combined with heat-reduction . Interestingly, the minimum reflection loss (RL_{min}) of the $NiFe_2O_4$/MXene composite was -13.3 dB, indicating much stronger EMW absorption properties than pure MXene nanosheets (RL_{min} = -7.03 dB) at the same loading. The presence of $NiFe_2O_4$ nanoparticles primarily accounts for the prevention of MXene nanosheets from self-stacking, thereby enhancing conduction loss.. In addition, the presence of MXene promotes the growth and organization of nickel ferrite nanoparticles, resulting in enhanced crystal structure and surface effect between nanoparticles and MXene sheets throughout the composite. More importantly, the magnetic loss generated by the magnetic $NiFe_2O_4$ nanoparticles is beneficial for good impedance matching, allowing more EMW to enter the composite for dissipation. This study opens up a promising approach to enhance the absorption properties of X-band electromagnetic waves.

Introduction

Electromagnetic waves (EMW) in the X-band (8–12 GHz) are essential to many modern technological applications, including advanced military and civilian radar systems, broadband satellite transmissions, and some wireless communications devices [1], [2]. Despite the many benefits, the prevalence of EMW in this frequency range also poses potential health concerns and potential interference to sensitive electronic devices, requiring careful monitoring and research [3]. The biggest challenge today is to optimize EMW absorption in the X-band to minimize negative impacts while maintaining high performance. Research has focused on developing materials with efficient broadband absorption capabilities, with the goal of achieving extremely low reflection loss (typically less than 10 dB) and strong wave attenuation [4]. To achieve this goal, scientists are exploiting advanced composite materials with tailored dielectric and magnetic properties. Optimizing the combination of loss mechanisms (e.g. dielectric and magnetic losses) along with wave impedance matching is key to achieving efficient electromagnetic wave energy

https://doi.org/10.62239/jca.2025.064

dissipation, contributing to safer EMW control and applications [5], [6]. Ti_3C_2 MXene, with the chemical formula $M_{n+1}X_nT_x$, is a class of two-dimensional (2D) materials that are attracting considerable attention as a promising multifunctional material. M stands for early transition metals such as Ti, V, Nb, and Mo, while X refers to Carbon, Nitrogen, or both; n can be 1, 2, or 3; and Tx denotes surface functional groups like O, OH, or F [7]. MXene possesses many excellent properties such as high electrical conductivity, unique layered structure, large surface area with many functional groups, intrinsic defects, and light weight [8]. Thanks to these properties, MXene has become a promising candidate for many high-tech applications, including supercapacitors, lithium-ion batteries, electrocatalysts, lithium-sulfur batteries, sensors, and photocatalysis [9], [10]. In particular, the properties of MXene also help to effectively reduce polarization loss and conduction loss, while enhancing the ability to reflect multiple electromagnetic waves (EMW). This makes MXene a novel dielectric loss-based EMW absorbing material with great application potential [11]. To achieve optimal EMW absorption performance, the material needs to have strong EMW attenuation ability and good impedance matching ability [12]. However, MXene also faces some significant challenges. The excessively high conductivity and/or complex dielectric constant of MXene can often lead to unwanted EMW reflection due to poor impedance matching between the MXene surface and air [13]. Furthermore, the self-stacking of MXene nanosheets also reduces the value of its unique 2D structure [14]. All these factors significantly affect the EMW absorption capacity of MXenes, thereby hindering their practical applications [13], [14]. Fortunately, the integration of crystalline phases with high magnetic loss is an effective strategy to expand the absorption bandwidth and improve the overall performance [15]. The functional groups on the material surface play a dual role: they not only influence the electromagnetic properties but also provide binding sites for surface decoration with other materials [16]. For example, the use of metal ions such as Ni^{2+} and Fe^{3+} to complex with the functional groups on the surface can facilitate the formation of magnetic spinel ferrite phases [17], [18]. The combination of the base absorbent material and magnetic ferrite layers offers significant potential to optimize the EMW absorption capacity in the X-band, improving both shielding performance and electromagnetic compatibility [19].

Nickel Ferrite ($NiFe_2O_4$) is known for its remarkable properties such as moderate saturation magnetization, soft magnetism, high chemical stability, good dielectric properties, and high-frequency magnetic resonance. These properties contribute to its ability to exhibit significant complex permeability values in the GHz frequency range. However, achieving large complex permeability of nickel ferrite can result in poor impedance mismatch and a monotonic loss mechanism. Furthermore, the magnetic and dielectric properties of nickel ferrite are significantly affected by its morphological structure and cation distribution, which may limit its electromagnetic wave absorption performance in some specific applications. To overcome these limitations, the dielectric and magnetic properties of nickel ferrite can be tuned and optimized by changing its composition, microstructure, or combining it with other materials (e.g. carbon, graphene, MXene). This method holds significant promise for greatly improving the electromagnetic wave (EMW) absorption capabilities of nickel ferrite, particularly across a broad frequency spectrum, thereby paving the way for new research avenues and applications in electromagnetic wave absorption materials, especially within the X-band.. In previous reports, Ti_3C_2 MXene was used to decorate the surface of nickel ferrite to enhance both impedance matching and EMW absorption properties. Yan Guo et al. successfully synthesized Ti_3C_2 MXene composites decorated with nickel ferrite nanoparticles by electrostatic self-assembly combined with freeze-drying, achieving an RL_{min} value of -41.38 dB with 3% $NiFe_2O_4$ content in a paraffin matrix [20]. Rui Zeng et al. synthesized nickel ferrite particles via in situ growth on MXene/carbon-nitrogen (MXene/CN)-based materials. The MXene/$NiFe_2O_4$/CN composite exhibited an impressive RL_{min} of -50.51 dB at 17.3 GHz with a thickness of 1.5 mm, with an effective absorption bandwidth of 4.95 GHz (13.02–18 GHz) [21]. Although previous studies have attempted to exploit the resonance effect of nickel ferrite and MXene to enhance the electromagnetic wave (EMW) absorption properties, achieving both a broad absorption frequency and strong absorption in the X-band for practical applications remains a significant obstacle. This suggests that finding the optimal solution for EMW absorption materials remains a challenge to be overcome.

In this study, nickel ferrite nanoparticles were grown in situ on the Ti_3C_2 MXene surface by a facile thermal treatment method. The MXene sheets served as a template for the in situ development of nickel ferrite

https://doi.org/10.62239/jca.2025.064

nanoparticles.. This templating effect effectively prevented the agglomeration of nanoparticles and promoted their uniform dispersion. Our study investigated the effect of varying the MXene content on the microstructure, magnetic properties, and X-band electromagnetic wave absorption characteristics of nickel ferrite/MXene composites.

Experiment

Chemicals

Titanium aluminum carbide (Ti_3AlC_2), Merck; Nickel (II) nitrate hexahydrate ($Ni(NO_3)_2.6H_2O$), Merck; Iron (III) nitrate nonahydrate ($Fe(NO_3)_3.9H_2O$), Merck; Hydrofluoric acid (HF), Xilong; Ammonia (NH_3), Merck; Paraffin, Xilong.

Preparation of materials

Ti_3C_2 MXene was produced through the HF etching technique [8]. First, 1 g of MXene powder was mixed into 100 mL of deionized water and magnetic stirred for 30 minutes. $Ni(NO_3)_2.6H_2O$ and $Fe(NO_3)_3.9H_2O$ were measured in a molar ratio of Ni^{2+}:Fe^{3+}=1:2 and dissolved in another 100 mL of deionized water. This salt solution was gradually introduced to the MXene dispersion over a period of 30 minutes. The pH of the mixture was adjusted to 10 by slowly adding a 25% NH_3 solution, followed by magnetic stirring for 2 hours. The mixture was then centrifuged and washed several times with deionized water until the pH was approximately 7. The resulting precipitate was dried under vacuum at 85°C for 24 hours. Finally, the sample was finely ground into a powder, placed in a ceramic cup, and heated to 500°C for 2 hours in a nitrogen atmosphere. The composite material obtained, containing Ti_3C_2 MXene at 0, 30, 50, 75, and 100 wt. %, was designated as NiFeO-MX-X, where X represents the weight percentage of Ti_3C_2 MXene.

Material characterization

The surface morphology and elemental composition of the samples were investigated using a Hitachi S-4800 scanning electron microscope (SEM), integrated with an energy-dispersive X-ray (EDX) analysis system at an acceleration voltage of 15 kV. The crystal structure of the $NiFe_2O_4$ - MX material was determined by X-ray diffraction (XRD) on a Bruker D8-Advance, using CuK radiation in the 2θ angle range from 10° to 70°. The static magnetic properties were measured using a vibrating sample magnetometer (VSM, DMS880).

For the electromagnetic wave (EMW) absorption measurements, sheet-shaped samples were prepared by dispersing 5% of $NiFe_2O_4$- MXene powder into molten paraffin wax. The mixture was then condensed in a mold with dimensions of 200x200x2 mm. EMW absorption performance was evaluated using a Keysight N9918A instrument.

Results and Discussion

The microstructures of pure MXene, $NiFe_2O_4$ and $NiFe_2O_4$-MXene composites are depicted in Figure 1.

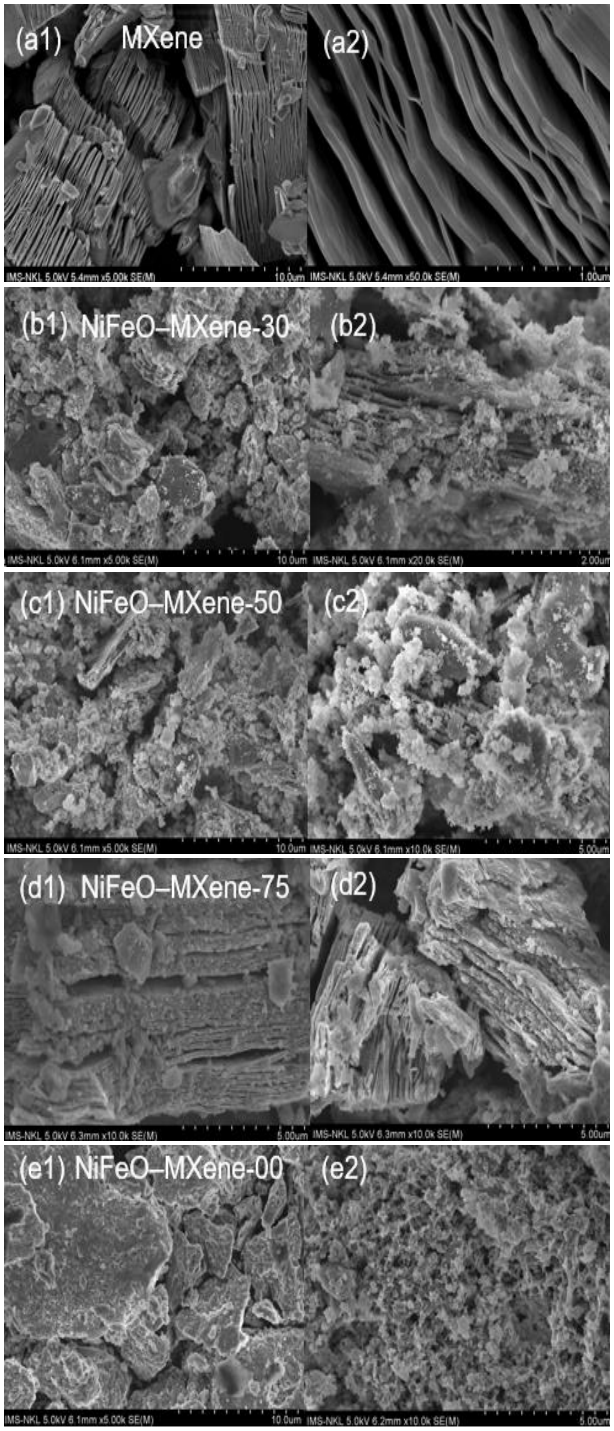

Fig. 1: SEM images of $NiFe_2O_4$-MXene composites with different MXene contents at different ratios (a1, a2)

https://doi.org/10.62239/jca.2025.064

Pure MXene; (b1, b2) 30 wt.%; (c1, c2) 50 wt.%; (d1, d2) 75 wt.%; (e1, e2) Pure $NiFe_2O_4$.

MXene is characterized by a typical accordion-like multilayer microstructure (Figure 1a). The pristine $NiFe_2O_4$ molecule has a relatively uniform particle (Figure 1e). Figure 1(b-d) illustrates the SEM images of the $NiFe_2O_4$-MXene composites. Compared with the severe agglomeration of pure $NiFe_2O_4$ shown in Figure 1e, the nanometer-sized $NiFe_2O_4$ nanoparticles are firmly and uniformly anchored on the surface or incorporated into the interlayers of MXene sheets without obvious agglomeration due to the steric hindrance, hydrogen bonding and electrostatic interactions, leading to improved dispersibility. The in situ growth of $NiFe_2O_4$ nanoparticles on the MXene surface may be due to the functional groups present in MXene, such as -OH, -O, and -F, which facilitate the particle formation. During heat treatment, $NiFe_2O_4$ nanoparticles crystallized uniformly on the surface or inside the interlayers of MXene sheets.

The EDS spectrum of the $NiFe_2O_4$-MXene composite materials is shown in Fig. 2.

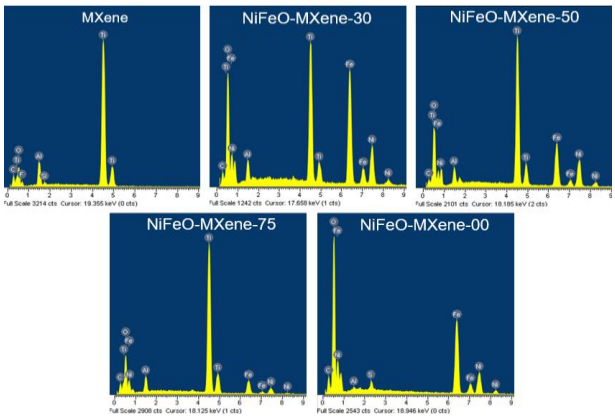

Fig. 2: EDS images of $NiFe_2O_4$-MXene composite materials

Table 1: EDS results of $NiFe_2O_4$-MXene composite materials at different MXene contents.

Sample	Ni (%)	Fe (%)	O (%)	Ti (%)	C (%)	Al (%)
NiFeO-MX-00	17,76	41,35	32,19	-	6,85	0,64
NiFeO-MX-30	12,13	24,98	38,12	16,99	5,82	5,82
NiFeO-MX-50	13,04	13,91	39,41	26,18	5,32	2,14
NiFeO-MX-75	3,62	5,89	43,58	36,35	8,23	2,32
MXene	-	-	32,13	44,01	10,93	4,12

The presence of characteristic peaks corresponding to Ni, Fe and O in the spectrum confirms the successful incorporation of nickel ferrite nanoparticles in the composites. As the MXene content increases, the corresponding Ti content in the composites is measured to be 16.99%, 26.18%, 36.35%, respectively.

XRD patterns of $NiFe_2O_4$, MXene, and $NiFe_2O_4$-MXene samples are shown in Fig. 3. The characteristic diffraction peaks at 2θ = 6.5°, 18.3°, and 38.0° correspond to the (002), (004), and (110) crystal planes of MXene ($Ti_3C_2T_x$) [23]. Meanwhile, the peaks at 30.2°, 35.5°, 43.1°, 53.5°, 57.0°, and 62.6° correspond to the (220), (311), (400), (422), (511), and (440) planes of the $NiFe_2O_4$ spinel phase [22], confirming the coexistence of the $NiFe_2O_4$ spinel phase and the MXene phase – the conductive matrix phase.

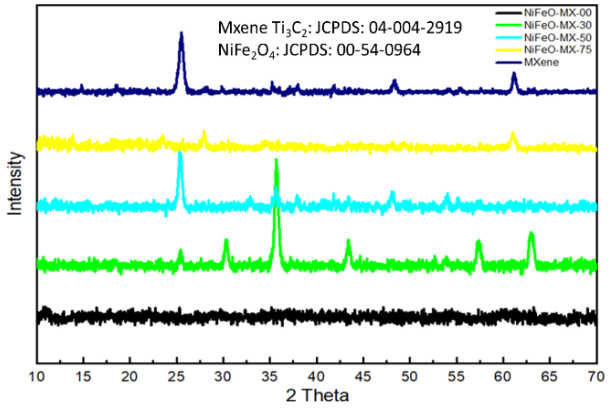

Fig. 3: X-ray diffraction (XRD) pattern of $NiFe_2O_4$-MXene composite material

Fig. 4 shows the magnetic hysteresis loops of the pristine $NiFe_2O_4$, MXene and $NiFe_2O_4$-MXene composites with different MXene mass ratios. From the synthesis results, it can be seen that increasing the $NiFe_2O_4$ mass ratio increased the saturation magnetic values for the composites from 0 emu/g (100 wt.% MXene) to 21.7 emu/g (30 wt.% MXene)

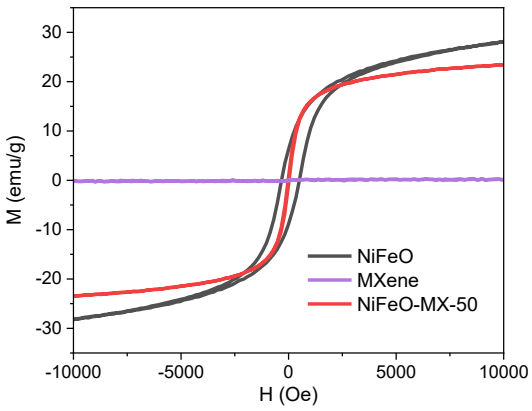

Fig. 4: Hysteresis loops of of $NiFe_2O_4$-MXene composites

https://doi.org/10.62239/jca.2025.064

The magnetic properties of $NiFe_2O_4$-MXene composites depend on many factors, including grain size, crystal domain structure, grain shape, lattice defects, presence of secondary phases, and surface/interface effects [23,24]. These factors play an important role in determining the magnetic behavior and characteristics of the composites. As the MXene content increases, the saturation magnetization decreases due to the non-magnetic nature of the MXene phase. This is consistent with the study of D. Shan et al. [26] because the magnetic properties of the material mainly come from $NiFe_2O_4$ - a magnetic ferrite. The magnetic hysteresis curve changes from a typical 'S' shape to a straight line near the origin, reflecting the change in magnetic structure. Therefore, when combining $NiFe_2O_4$ and MXene together, we can adjust the saturation magnetization index (Ms) of the composites.

Fig. 5 depicts the frequency-dependent reflection loss in the X-band for the $NiFe_2O_4$-MXene sample with varying MXene content. Pure MXene Ti_3C_2 exhibits weak EWM absorption performance, reaching -7.03 dB. Pure nickel ferrite exhibits stronger EMW properties than MXene in the X-band with an RLmin of -11.1 dB and an EAB of 0.5 GHz. When MXene is modified with $NiFe_2O_4$, the absorption capacity of MXene is significantly increased. Increasing the MXene content to 30 wt.% results in an RLmin of -10.98 dB and an EAB of 1.1 GHz. Furthermore, increasing the MXene content shows excellent EMW absorption performance at 50 wt.% MXene Ti_3C_2 content with an RLmin of -13.3 dB and an EAB of 1.6 GHz.

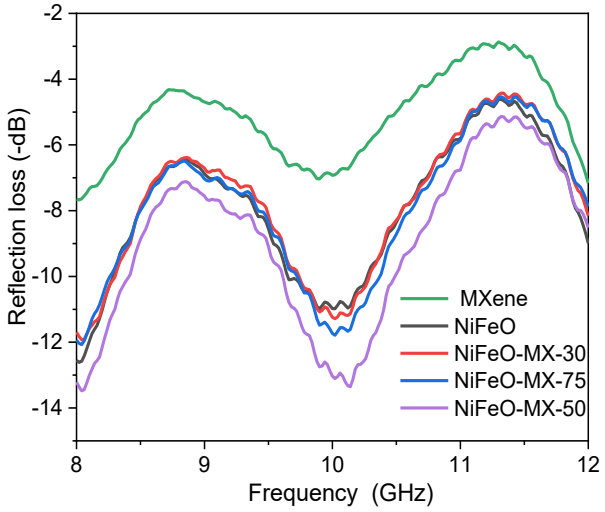

Fig. 5: Reflection loss curves of $NiFe_2O_4$-MXene composites

The change in EMW absorption properties can be mainly attributed to the difference in the electromagnetic properties of the materials arising after the incorporation of MXene with $NiFe_2O_4$. These results demonstrate that the amount of MXene and $NiFe_2O_4$ when incorporated has a significant impact on the EMW absorption properties of the nano-composites and thus needs to be well optimized. Based on the different electromagnetic wave absorption mechanisms and the unique properties of different types of wave absorption materials, MXene has so far been successfully incorporated with many materials to fabricate electromagnetic wave absorption composites, such as carbon nanotubes, graphene, metals (metal oxides) and conducting polymers, which can correspond to different electromagnetic wave loss mechanisms and can effectively adjust the impedance matching and enhance the electromagnetic wave absorption ability. In addition, by designing different microstructures and macromorphologies, the wave absorption performance of MXene-based composites can also be enhanced. Therefore, the synthesized NiFe2O4-Mxene composites have promising practical applications as high-performance electromagnetic wave absorbers in the X-band range.

Conclusion

The nickel ferrite/Ti_3C_2 MXene composite material was easily synthesized through a heat treatment method. This process allows cobalt ferrite nanoparticles to grow directly on the surface and intercalate into the layers of the MXene sheet, creating a unique structure. This structure not only optimizes the grain size effect but also enhances the surface effect between nikel ferrite and MXene throughout the material. As a result, the electromagnetic properties of the composite material are significantly improved, resulting in superior X-band electromagnetic wave absorption. Specifically, pure MXene Ti_3C_2 shows a minimum reflection loss of -7.03 dB and an effective absorption bandwidth of almost 0 GHz. With 50 wt% Ti_3C_2 MXene addition, the nickel ferrite/MXene composite achieved an impressive minimum reflection loss of -13.3 dB at 10.02 GHz, along with an effective absorption bandwidth of 1.6 GHz.

Acknowledgement

This research was funded by Science and Technology Development Project Number 10/2025/HĐKHCN.

https://doi.org/10.62239/jca.2025.064

References

1. R.J. Doviak, D.S. Zrnić, Doppler Radar and Weather Observations, 2nd ed., Courier Corporation, 1993.
2. T.S. Rappaport, Wireless Communications: Principles and Practice, 2nd ed., Prentice Hall PTR, 2002.
3. IEEE Committee on Man and Radiation, IEEE Standard for Safety Levels with Respect to Human Exposure to Radio Frequency Electromagnetic Fields, 3 kHz to 300 GHz, IEEE Std C95.1-2005 (2005).
4. X. Wang, C.F. Liu, H. Chen, W.S. Lu, N.S. Bao, C.X. Xu, Adv. Mater. Interfaces, 6(19) (2019) 1900595. https://doi.org/10.1002/admi.201900595
5. L. Li, M. Zhang, J. Zhang, J.S. Wu, Compos. Part B Eng., 200 (2020) 108304. https://doi.org/10.1016/j.compositesb.2020.108304
6. C.K. Lee, S.S. Lee, J. Magn. Magn. Mater., 320(18) (2008) 2486-2490. https://doi.org/10.1016/j.jmmm.2008.04.049
7. B. Anasori, M.R. Lukatskaya, Y. Gogotsi, Nat. Rev. Mater., 2(2) (2017) 16098. https://doi.org/10.1038/natrevmats.2016.98
8. Y. Gogotsi, B. Anasori, ACS Nano, 13(9) (2019) 9680-9685. https://doi.org/10.1021/acsnano.9b06394
9. M. Alhabeb, K. Maleski, B. Anasori, P. Lelyukh, L. Clark, S. Sin, Y. Gogotsi, Chem. Mater., 29(18) (2017) 7620-7633. https://doi.org/10.1021/acs.chemmater.7b02847
10. R.B. Rakhi, P.K. Nayak, B. Anasori, M. Ghidiu, Y. Gogotsi, H.N. Alshareef, ACS Appl. Mater. Interfaces, 8(40) (2016) 26814-26820. https://doi.org/10.1021/acsami.6b08389
11. M. Han, J. Yan, Y. Li, S. Liang, P. Liu, J. Mater. Chem. C, 8(28) (2020) 9477-9494. https://doi.org/10.1039/D0TC01822H
12. M.S. Cao, J.C. Shu, X.Y. Fang, S.Y. Zhao, J. Zhang, Adv. Mater. Technol., 5(5) (2020) 1901026. https://doi.org/10.1002/admt.201901026
13. Z. Wang, S. Li, W. Zhang, F. Chen, J. Wang, Y. Yang, H. Dong, J. Mater. Sci. Technol., 51 (2020) 268-283. https://doi.org/10.1016/j.jmst.2020.03.047
14. X. Liu, S. Du, H. Li, X. Zhao, C. Xu, S. Zhang, J. Mater. Sci., 56(29) (2021) 16407-16430. https://doi.org/10.1007/s10853-021-06325-2
15. N. Sharma, S. Arya, M. Lal, Spinel and Inverse Spinel Ferrites for Microwave Absorption, in: Spinel and Inverse Spinel Ferrites, Chapman and Hall/CRC, 2025.
16. Q. Wang, J. Li, P. Zhang, Mater. Today Nano, 22 (2023) 100278. https://doi.org/10.1016/j.mtnano.2023.100278
17. Y. Liu, X. Wang, Y. Chen, J. Alloys Compd., 848 (2020) 156553. https://doi.org/10.1016/j.jallcom.2020.156553
18. R. Kumar, V.K. Yadav, V.P. Singh, Ceram. Int., 47(11) (2021) 15488-15495. https://doi.org/10.1016/j.ceramint.2021.02.115
19. W. Sun, Z. Liu, J. Gao, Compos. Part B Eng., 235 (2022) 109786. https://doi.org/10.1016/j.compositesb.2022.109786
20. Y. Guo, D. Lan, J. Liu, X. Zhao, X. He, Q. Ren, Adv. Compos. Hybrid Mater., 4(3) (2021) 602-613. https://doi.org/10.1007/s42114-021-00279-0
21. R. Zeng, Z. Zhang, Y. Yang, J. Yan, X. Zhang, Molecules, 28(1) (2023) 233. https://doi.org/10.3390/molecules28010233
22. S. Anwar, M. Ahmed, B. Murtaza, M.S. Khan, M.A. Khan, J. Magn. Magn. Mater., 511 (2020) 166943. https://doi.org/10.1016/j.jmmm.2020.166943
23. J. Zhang, H. Yu, M. Han, Z. Zhou, C.M. Aguilar, J.S. Wu, Nanoscale Res. Lett., 13 (2018) 343. https://doi.org/10.1186/s11671-018-2746-4
24. Y.N. Pham, S.S.A. Shah, M.T. Do, RSC Adv., 10(52) (2020) 31622-31661. https://doi.org/10.1039/D0RA05133K
25. W. Sun, X. Li, J. Gao, J. Supercond. Nov. Magn., 34 (2021) 1477-1483. https://doi.org/10.1007/s10948-020-05718-5
26. D. Shan, S. Wu, J. Yang, Results Phys., 15 (2019) 102750. https://doi.org/10.1016/j.rinp.2019.102750
27. X. Su, J. Wang, J. Wang, J. Mater. Sci. Mater. Electron., 32(6) (2021) 6881-6894. https://doi.org/10.1007/s10854-021-05273-2
28. Y. Tian, Z. Liu, H. Wang, J. Alloys Compd., 967 (2023) 171796. https://doi.org/10.1016/j.jallcom.2023.171796
29. J. He, S. Liu, L. Deng, J. Kong, Appl. Surf. Sci., 504 (2020) 144210. https://doi.org/10.1016/j.apsusc.2019.144210
30. D.P. Siva Nagasree, R.B.R. Krishna, M.C. Rao, Plast. Rubber Compos., 50(2) (2021) 71-82. https://doi.org/10.1080/14658011.2020.1836882
31. Mashuri, S. Pratapa, Mater. Res. Express, 5(1) (2018) 014003. https://doi.org/10.1088/2053-1591/aa68b4
32. S. Mohammad, F. Khan, M.U. Islam, J. Mater. Sci. Mater. Electron., 30 (2019) 2278-2284. https://doi.org/10.1007/s10854-018-0498-7
33. S.H. Ismail, S.I. El-Dek, S.A. Sabry, Appl. Phys. A, 124 (2018) 420. https://doi.org/10.1007/s00339-018-1808-x
34. P. Liu, J. Kong, J. Mater. Sci., 55 (2020) 10339-10350. https://doi.org/10.1007/s10853-020-04739-8
35. P. Liu, V.M.H. Ng, Z. Yao, Mater. Lett., 229 (2018) 286-289. https://doi.org/10.1016/j.matlet.2018.07.045
36. Z. Wang, G.H. Dong, J. Mater. Sci. Mater. Electron., 30 (2019) 15250-15256. https://doi.org/10.1007/s10854-019-01897-7